ELSEVIER

Contents lists available at ScienceDirect

Combustion and Flame

journal homepage: www.elsevier.com/locate/combustflame



3D printed ABS/paraffin hybrid rocket fuels with carbon dots for superior combustion performance



Cagri Oztan^{a,*}, Eric Ginzburg^{a,1}, Mert Akin^{a,1}, Yiqun Zhou^b, Roger M. Leblanc^b, Victoria Coverstone^a

- ^a Department of Mechanical and Aerospace Engineering, University of Miami, Coral Gables, FL 33146, USA
- ^b Department of Chemistry, University of Miami, Coral Gables, FL 33146, USA

ARTICLE INFO

Article history:
Received 8 May 2020
Revised 5 November 2020
Accepted 12 November 2020
Available online 27 November 2020

Keywords:
Hybrid rockets
Additive manufacturing
Regression rate
Combustion
Carbon
Dots

ABSTRACT

In this research, the combustion performance of a novel, composite hybrid rocket fuel grain composed of Acrylonitrile Butadiene Styrene (ABS) and Paraffin was investigated to understand the effects of incorporation of a novel nanomaterial: gel-like carbon dots (CDs), into the paraffin component. ABS fuel grains with straight ports were 3D printed and used as molds into which base and 1 wt% CD-loaded paraffin materials were casted separately. For control, pure ABS fuel grains were also printed. All fuel grains were exposed to ballistic tests using the lab-scale test setup where gaseous oxygen (GOX) was employed as oxidizer. Test results exhibited that ABS/CD-loaded paraffin fuel grains manifested a maximum combustion efficiency and regression rate of 88% and 1.29 mm/s, which marked enhancements of about 8.5% and 11% compared to ABS/pure paraffin fuel grains, respectively. Despite the compromise in the mechanical properties, the enhancement in combustion characteristics of CD-loaded fuel grains was attributed to lower viscosity, higher particle entrainment, specific surface area and catalytic activity

© 2020 The Combustion Institute. Published by Elsevier Inc. All rights reserved.

1. Introduction

Hybrid rocket systems combine the inherent advantages of solid fuels and liquid propellants, which renders them highly manufacturable, inexpensive and less sophisticated than other rocket systems. Hybrid rockets offer increased safety due to the distinct physical states of the fuel and oxidizer, on-demand thrust, reduced environmental impact and low cost fabrication, which make them a suitable option for applications such as suborbital flight missions [1].

Despite these advantages, a potential large-scale utilization of hybrid rockets is hindered by low regression rates due to the classical diffusion flame-limited combustion [2–4]. Commonly employed solid fuels such as hydroxyl terminated polybutadiene (HTPB) are known to have low regression rates due to this boundary layer combustion mechanism. In order to address these short-comings, several structural modification strategies such as intricate port geometries, opposed fuel burners and impinging injectors have been investigated so far [5–17]. To attain further enhancement in combustion properties, Karabeyoglu et al. investi-

gated long-chained hydrocarbon fuels such as paraffin, in which non-classical hybrid combustion where the formation of a low-viscosity liquid layer on the fuel surface is observed [18]. In this type of combustion, droplets of liquified fuel grain are entrained into the gas stream, thereby ensuring higher levels of mass transfer [19,20]. Karabeyoglu et al. also theorized that the rate of entrained mass in liquefying fuels is inversely proportional to the viscosity and suggested the following correlation [18]:

$$\dot{m}_{ent} \propto \frac{P_d^a h^{\beta}}{\mu_l^{\gamma} \sigma^{\pi}}$$
 (1)

where P_d , h, μ_l and σ are dynamic pressure, melt layer thickness, viscosity and surface tension, respectively, with α , β , γ and π being empirical constants. Due to the aforementioned prominence of viscosity in combustion properties, several strategies aiming to reduce it via incorporation of nano or micro additives have been investigated so far. Chen et al. studied the effect of multi-walled carbon nanotubes (MWCNT) on the regression rate of HTPB where an increase in thermal conductivity and regression rate for an optimal MWCNT mass ratio of 1% were reported [21]. Akhter et al. utilized lithium aluminum hydride (LiAlH₄) and magnesium hydride (MgH₂) nanoparticles with paraffin-based fuels and achieved 3.5–4.75 fold enhancement in regression rate [15]. Kobald et al. studied the effect of adding nanoclay in the paraffin matrix upon which

^{*} Corresponding author. E-mail address: cyo4@miami.edu (C. Oztan).

¹ †These authors contributed equally.

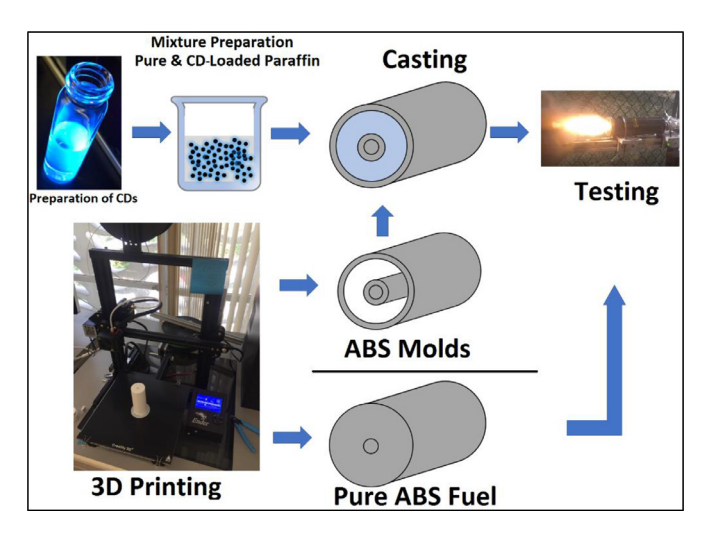


Fig. 1. The multi-step experimental strategy followed in this research.

appreciable improvement in combustion properties due to reduction in viscosity was reported [22].

Carbon quantum dots (CDs), are a class of unique carbon-based nanomaterials that were serendipitously discovered in 2000's and have undergone significant development since 2004. CDs were reported for the first time by Xu et al. when single-walled carbon nanotubes (SWCNT) were tentatively purified by arc-discharge soot followed by electrophoresis which manifested new bright spots due to the presence of CDs [23]. CDs possess many characteristic advantages such as small particle size (less than 10 nm), excellent photoluminescence (PL), good biocompatibility, non-toxicity and abundant surface functionalities [24-26]. Up to now, CDs have been successfully utilized for various purposes such as drug delivery, nanomedicine, stereolithography 3D printing, photocatalvsis, thermoelectric energy conversion, sensing and bioimaging [27-32]. CDs were also demonstrated to increase thermal conductivity in phase change materials [33], enhance combustion efficiency with mitigated emissions in diesel engine fuels by triggering better air/fuel mixing [34] and possess low viscosity due to their anionic nature [35,36], which make them an excellent candidate for augmenting combustion properties of fuel grains.

In this research, we report a novel composite hybrid rocket fuel grain fabricated via additive manufacturing of Acrylonitrile Butadiene Styrene (ABS), followed by casting of paraffin loaded with a unique class of CDs, gel-like CDs, into it. As opposed to the numerous previously reported research studies concerning additively manufactured hybrid rocket fuel grains with intricate port geometries [37–39], the main focus of this research is the investigation of the effect of gel-like CDs on combustion properties of a solid fuel grain with straight port. Ballistic properties of each type of fuel grain were correlated with microstructural, rheological and thermal properties.

2. Materials and methods

The multi-step experimental strategy as illustrated in Fig. 1 was followed to fabricate three different types of fuel grains. In novel grains, gel-like CDs were fabricated and mixed with paraffin. For control, both ABS/paraffin and pure ABS fuel grains were also fabricated, the latter being fully 3D printed.

2.1. Preparation of gel-like CDs

The materials used to synthesize and purify gel-like CDs were reported in [40]. Initially, 5 mL of 1,2-ethylenediamine (EDA)

(>99.0%, MP Biomedicals, Irvine, CA, USA) was transferred into a 50 mL round-bottom flask with argon flux (ultra-high purity, Airgas, Miami, FL, USA) which lasted for 5 min and heated with constant stirring in an oil bath on a hot plate (Chemglass, OptiMag-st). When the temperature reached 160 °C, 1 g of citric acid (99.5-100%, VWR, West Chester, PA, USA) was added with vigorous stirring. The reaction sustained for 50 min until complete dissolution of citric acid in EDA was ensured. Argon gas was applied through the whole reaction to prevent EDA from oxidizing. After cooling the system for 15 min down to room temperature, gel-like CDs formed at the bottom of the flask. The remaining unreacted EDA supernatant was then extracted three times using 10 mL acetone (99.9%, VWR, West Chester, PA, USA) and discarded. Subsequently, 0.8 g of gel-like CDs was dispersed in 1 mL of deionized water, which was later processed by vacuum evaporation at a constant temperature of 70-80 °C. The deionized water was purified by a Modulab 2020 water purification system from Continental Water System Corporation (San Antonio, TX, USA), which had a pH of 6.62 \pm 0.30, surface tension of 72.6 mN m⁻¹ and resistivity of 18 M Ω cm at 25.0 \pm 0.5 °C. All chemicals were used without further treatment.

2.2. Fuel grain fabrication

Three different types of fuel grains were fabricated with straight port. Initially, pure ABS fuel grains were 3D printed. Subsequently, composite fuel grains consisting of ABS and paraffin were fabricated. Each sample had a standard length of 60 mm. Cross-sectional dimensions of each fuel grain are shown in Fig. 2.

In all fuel grains, ABS component was 3D printed using a commercial ABS filament supplied by Hatchbox as feed stock for a Creality Ender 3D printer where a nozzle with a diameter of 1 mm was employed. In the slicing software, raft feature was activated to ensure better adhesion onto the build plate. To further enhance adequate adhesion on the heated bed, double sided tape was applied. For the ABS/paraffin fuel grains, paraffin blocks (supplied by MilliporeSigma) were heated up to 110 °C, right below the softening temperature of ABS to prevent deformation during casting. For the CD-doped novel fuel grains, paraffin was mixed with gel-like CDs at a ratio of 1% by mass upon melting. In both ABS/paraffin and CD-doped novel fuel grains, the approximate weight ratio of ABS-to-paraffin was maintained at 2:1. Fuel grains were ready for ballistic testing once the casted paraffin cooled down to room temperature. On average, all fuel grains weighed 52 g and took a total of 2 h to fabricate.

2.3. Ballistic testing and data acquisition

The lab-scale test setup as shown in Fig. 3 was constructed to perform ballistic tests. A flow system was designed to control and deliver the oxidizer, gaseous oxygen, to the combustion chamber. In each test, the feed pressure was adjusted using a brass CGA-540 hand operated regulator (HOV-1) with a 0–400 psi range. The solenoid valve (SOV-1) enabled the remote open and shutoff of oxidizer flow during tests, whereas the check valve (CV-1) also prevented contaminants or reactants from flowing upstream of the system. Several measurements were recorded in order to characterize the performance of the hybrid rocket and the fuel. These measurements included oxidizer mass flow, pressure, and temperature.

Pressure was measured at the inlet of the combustion chamber with an Omega SV121 (PT-1) with a measurable range of 0–1000 psi. The temperature of the combustion chamber was recorded using a k-type Omega thermocouple positioned at the top of the combustion chamber. Throughout the burning process, the oxidizer mass flow rate was measured with an Omega 1728A 0–500 SLM flow meter (FM-1). The pressure transducer operated

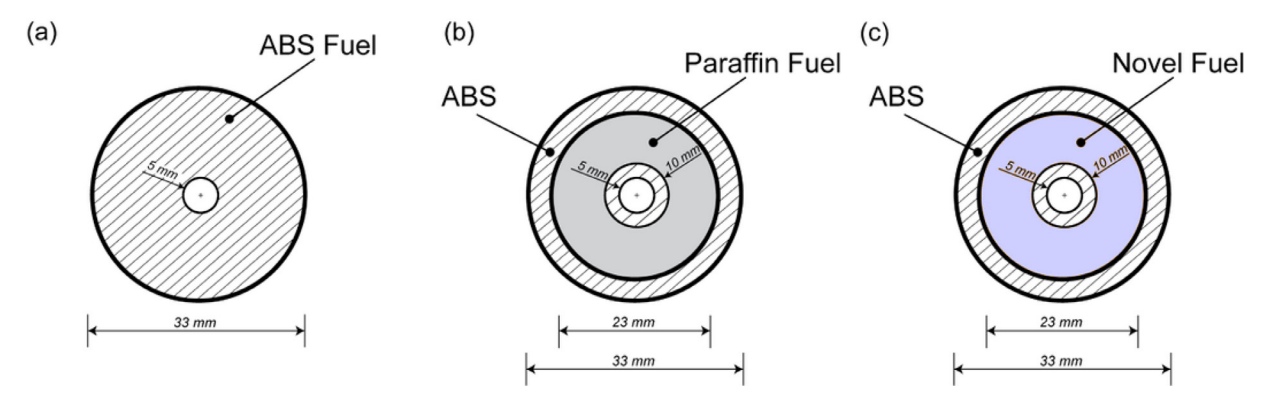


Fig. 2. Cross-sectional dimensions of each fuel grain: (a) ABS; (b) ABS - pure paraffin; (c) CD-doped novel fuel.

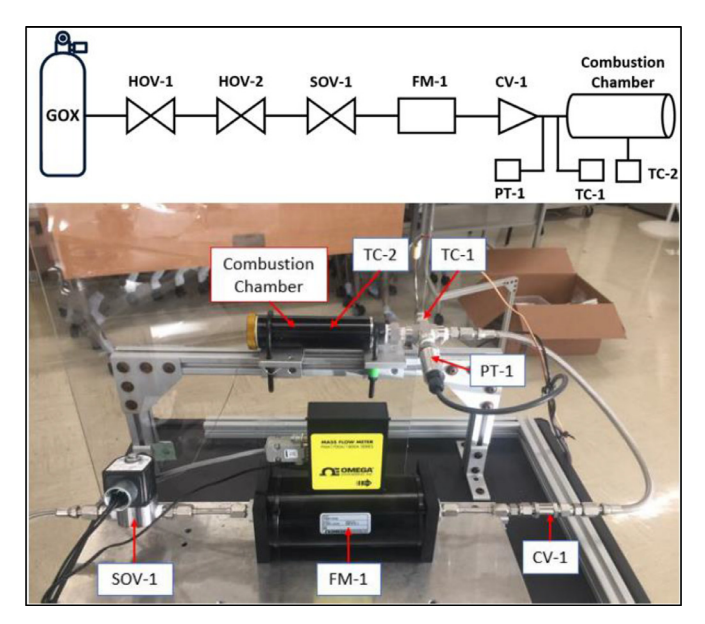


Fig. 3. Experimental ballistic test setup.

between 5 and 30 V DC of power and was supplied by 18 V DC using a portable battery pack. The flow meter was powered by a 12 V DC adapter. The variable DC power supply and the 12 V DC adapter were supplied by 110 V AC from a standard outlet source. The solenoid valve was also powered directly by 110 V AC with an integrated switch for remote operation. Finally, data acquisition was performed using a National Instruments Compact DAO Chassis cDAQ-9178 housing an NI-9219 C Series Universal Analog Input Module. All sensors were recorded at the same sample rate of 10 Hz. Initially, in the tests, an aluminum-based combustion chamber was used. Yet, due to the high pressure levels occurring during the tests, a thicker stainless-steel combustion chamber with a diameter of 33.1 mm was machined for use. A conical nozzle with a diameter of 5 mm was employed. Each test was initiated manually using an ignition wire and conducted in the same sequence as summarized in Table 1.

2.4. Evaluation of combustion performance

Characterization of the regression rate was initially performed using the following Eq. (2) below:

$$\dot{\mathbf{r}} = a\mathbf{G}_{\mathrm{ox}}^{\mathrm{n}} \tag{2}$$

The variables \dot{r} and G_{ox} denote regression rate and oxidizer mass flux, respectively. The terms a and n are the constants used

Table 1 Sequential control of each test.

Sequence	Time (s)	Action
1	0.0	Turn on data acquisition
2	5.0	Ignite the wire
3	8.0	Open SOV-1
4	18.0	Close SOV-1
5	23.0	Turn off PT-1
6	25.0	Turn off data acquisition

for exponential fitting of the data. Since the fuels comprised two different materials, regression rate for each component was determined iteratively. Because paraffin and ABS inherently possess distinct regression rate values and burning time, regression rate characterization for paraffin had to be performed by taking the significant O/F transition into the account. Thus, for more accurate results, the mass balance method given in Eq. (3) was used for regression rate calculations for paraffin-based fuels [40]:

$$\dot{\mathbf{r}}(\mathbf{t}) = \frac{\Delta m}{\rho_f \cdot \Delta t_b \cdot A_b} \tag{3}$$

where, for each component of the fuel, Δm is the burnt mass, ρ_f is the density, Δt_b is the burn time and A_b is the surface area on which regression occurs. Combustion efficiency was determined by the ratio of calculated and theoretical average characteristic velocities. The theoretical component was computed using NASA CEA software [41], whereas the experimental data was estimated using Eq. (4).

$$C^* = \frac{P_c A}{\dot{m}} \tag{4}$$

The parameters A, P_c and \dot{m} represent the fuel port area, average combustion chamber pressure and average mass flow rate, respectively.

2.5. Imaging, rheological, mechanical and thermal characterization

With the aim of making correlations between fabrication process and combustion performance, scanning electron microscopy (SEM), transmission electron microscopy (TEM), viscosity and thermal conductivity characterizations were performed. A Jeol JSM-5600 LV scanning electron microscope was used for microstructural imaging. The samples were mechanically loaded until failure and the specimen cross-sections were sputter coated with Au to prevent overcharging of the sample. The surface morphology of the CDs was investigated using a JEOL 1200X TEM device where a drop of CDs aqueous dispersion was deposited on a carbon-coated copper grid with subsequent air drying. In order to understand the effect of incorporation of CDs in paraffin, compressive strength of both type of samples also have been measured

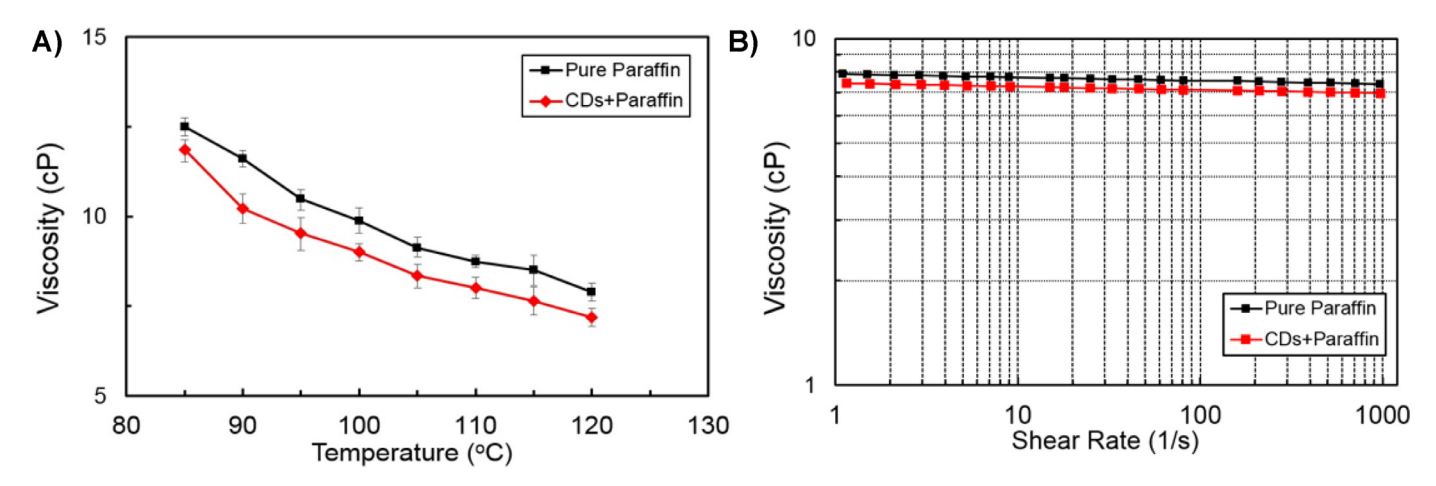


Fig. 4. Rheological properties of the paraffin samples. (a) Variation with temperature, (b) Variation with shear rate under 120 °C.

using an InstronTM 5966 universal testing frame in accordance with ASTM D575-91. Thermal conductivity measurements were carried out via transient hot-wire method using k-type thermocouples. Rheological characterization was conducted using a Haake RheoStress 6000 rotational rheometer under the constant temperature of 120 °C and between the temperature range of 85–120 °C. Finally, thermogravimetric (TGA) characterization of base paraffin and CD-doped paraffin samples was carried out using TG 209 F3 Tarsus at a heating rate of 10 °C/min.

3. Results

The rheological properties of each paraffin formulation with respect to temperature and shear rate are provided in Fig. 4a and b. Since ABS remains solid within the aforementioned temperature range, its viscosity data was excluded. Figure 4a displays the variation of viscosity in both neat and CD-loaded paraffin over the temperature range of 85–120 °C. The reduction in viscosity is more pronounced in the CD-loaded paraffin samples. The viscosity range recorded for pure paraffin and CD-loaded paraffin samples were 12.49–7.91 and 11.85–7.20 cP, respectively. On the other hand, Figure 4b represents the variation of aforementioned viscosity as a function of shear rate under 120 °C. Under constant temperature, pure paraffin samples manifested Newtonian behavior since the viscosity remained mainly constant with respect to shear rate.

SEM images of ABS and CD-doped paraffin fuel grains are provided in Fig. 5a and b. According to the SEM analysis, both materials exhibited porous structure. The porosity in ABS matrix can be attributed to the process-induced limitations of 3D printing such as poor infusion of the thermoplastic within the interface, warping in the matrix upon deposition onto the build plate and subsequent cooldown; whereas the porosity in the paraffin ensued due to the cooldown upon casting. The brittleness of paraffin also contributed to the formation of porosity. In comparison, the defects in the ABS matrix were observed to be significantly larger than those of the paraffin matrix. Gel-like CDs formed homogeneously distributed aggregates within the paraffin matrix, indicating sufficient mixing during the casting operation. The TEM image of gellike CDs and size distribution of 100 pristine dots are provided in Fig. 5c and d, respectively. The TEM micrograph demonstrated adequate dispersion with minimal aggregation and minor variations in the CD size. The gel-like CDs exhibited quasi-spherical geometry with a narrow Gaussian size distribution between 3.0 and 3.5 nm. The CDs had a high specific surface area up to $15-20 \text{ m}^2/\text{g}$.

SEM analysis also suggests that the compactly interconnected and regularly distributed aggregates of gel-like CDs may provide

better thermally conductive paths which agrees with the thermal conductivity data shown in Fig. 6a. Hierarchical increase in thermal conductivity shows that CD-loaded paraffin matrix possessed a 20% higher thermal conductivity of 0.30 W/m.K, compared to the 0.25 W/m.K of pure paraffin. Meanwhile, ABS matrix possessed the lowest thermal conductivity of 0.18 W/m.K. Figure 6b represents the thermogravimetric analysis results of each type of paraffin samples. The pure paraffin sample exhibited single-step decomposition after around 200 °C, whereas the doped paraffin sample was observed to decompose around 180 °C. This can be attributed to the increased thermal conductivity due to the presence of CDs, which increases the initial surface temperature, leading to higher regression rates and combustion efficiency. Finally, the compressive strength of each type of paraffin sample used in this research have been provided in Supplementary Fig. 1, where addition of 1 wt% CDs has been observed to reduce the compressive strength by 5%, from 3.54 MPa to 3.37 MPa.

Figure 7 displays the typical variations of combustion chamber pressure, surface temperature and mass flow rate. In all tests, pressure values were observed to reach a peak followed by a fluctuating trend due to the increase in the volume of the chamber caused by regression of the fuel. The transitions from ABS to paraffin and vice versa were observed to cause sudden changes in the combustion chamber pressure. The highest maximum surface temperature of 250 °C was attained by the CD-doped novel fuel grain, whereas ABS/paraffin and pure ABS grains exhibited the maximum surface temperatures of 210 and 120 °C, respectively.

Variation of regression rate with average oxidizer mass flux is displayed in Fig. 8(a). Regardless of the presence of gel-like CDs, all paraffin samples exhibited complete burning in the primary ABS port. Due to the particle entrainment phenomenon, paraffin samples manifested higher regression rates compared to the fully printed pure ABS fuel grains. However, CD-loaded ABS + paraffin samples exhibited higher regression rates. The difference in regression rate due to the addition of gel-like CDs became more pronounced in higher values of oxidizer mass flux. CD-loaded fuel grains attained a highest regression rate of 1.29 mm/s, whereas the maxima of ABS/paraffin and pure ABS samples were 1.14 and 0.90 mm/s, respectively. Compared to ABS/paraffin and pure ABS fuel grains, CD-doped novel fuel grains demonstrated average improvements in regression rate by 8.5 and 83%, respectively. Exponential curve-fitting yielded Eqs. (5) to (7) for each type of sample:

$$\dot{r}_{novel} = 0.3173x^{0.2736} \tag{5}$$

$$\dot{r}_{ABS/Paraffin} = 0.4377x^{0.1828} \tag{6}$$

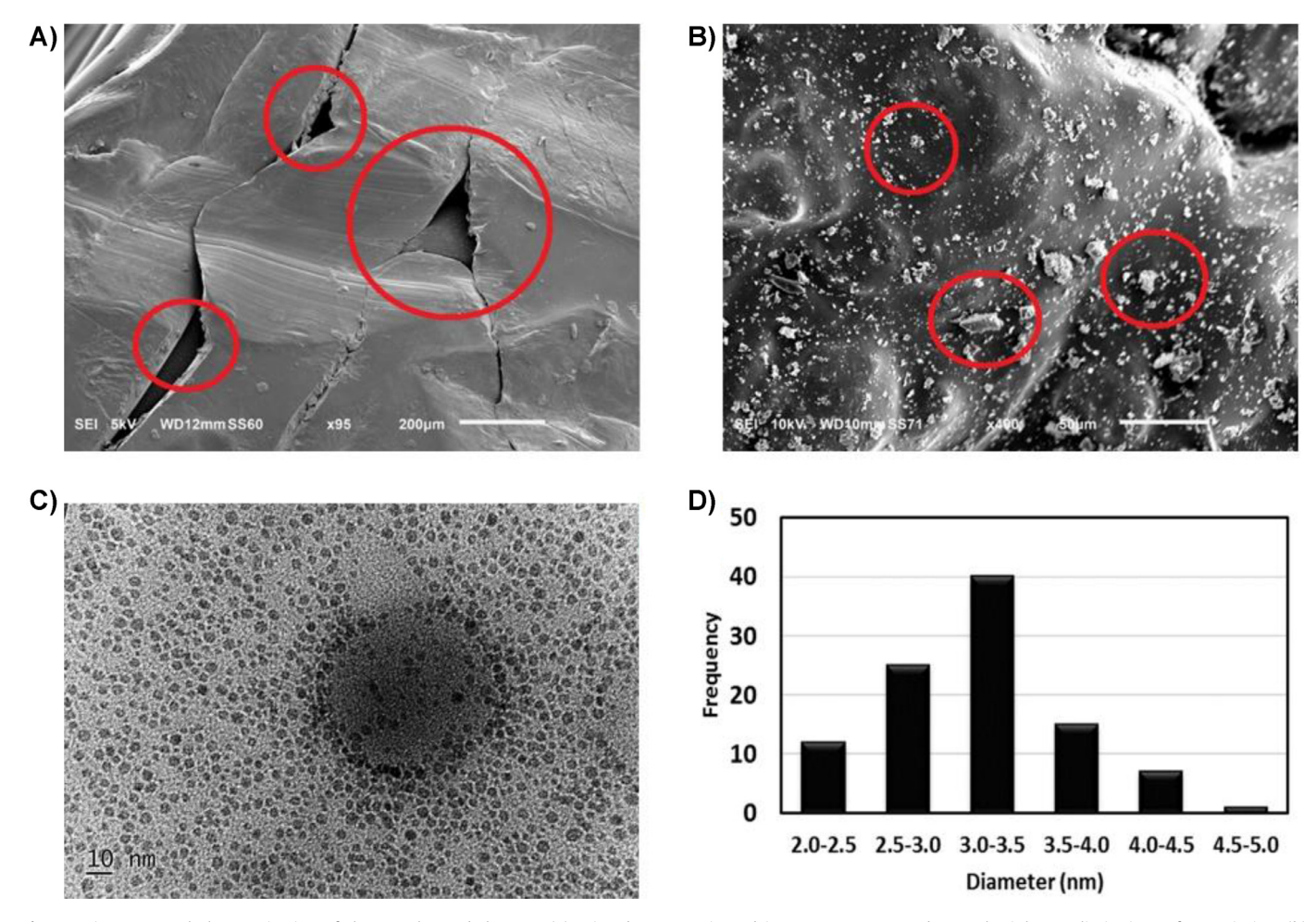


Fig. 5. Microstructural characterization of the samples and the CDs. (a) Printed ABS matrix and its porous structure due to the inherent limitations of 3D printing, (b) Aggregates of gel-like CDs within the paraffin matrix, (c) TEM micrograph of as-synthesized gel-like CDs, (d) Particle size distribution of gel-like CDs upon synthesis.

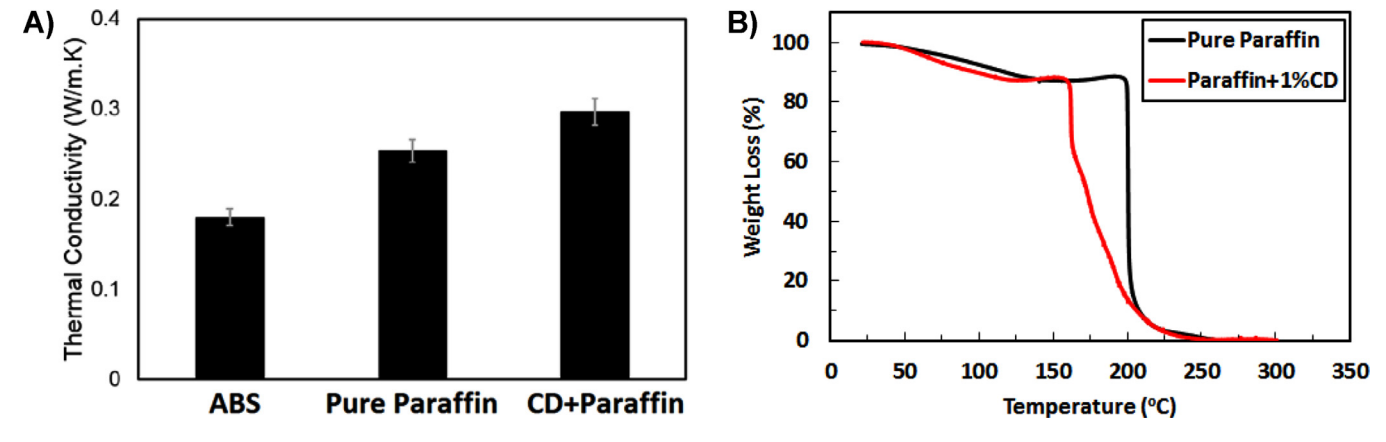


Fig. 6. Thermal characterization of the samples: (a) Thermal conductivity, (b) Thermogravimetry.

$$\dot{r}_{Pure\ ABS} = 0.1267x^{0.3728} \tag{7}$$

Calculated combustion efficiency data using the average pressure values in the middle of the combustion phase is provided in Fig. 8(b) where the solid lines identify the theoretical characteristic velocities for paraffin-based samples and the dashed line indicates the same for ABS samples. Per this figure, addition of gellike CDs in the paraffin matrix enhanced the combustion efficiency by an average of 7%. The highest combustion efficiency attained is 87% with CD-loaded fuels at an oxidizer-to-fuel ratio (O/F) of 1.384. The ranges of combustion efficiency are 80–87% for CD-loaded fuel

grains, 73–83% for ABS/paraffin composite fuel grains and 66–76% for pure ABS samples.

The enhancement in the combustion properties of the paraffin due to the addition of CDs can be attributed to certain mechanisms. Generally, paraffin-based hybrid rocket fuel grains suffer from low combustion efficiency, due to the insufficient vaporization during regression of the fuel which leaves behind high masses of paraffin unburned. Higher catalytic activity due to the presence of CDs was observed to cause higher levels of radiant heat transfer, shortened ignition delay and faster decomposition of the fuel as corroborated by TGA and ballistic tests, which are beneficial to

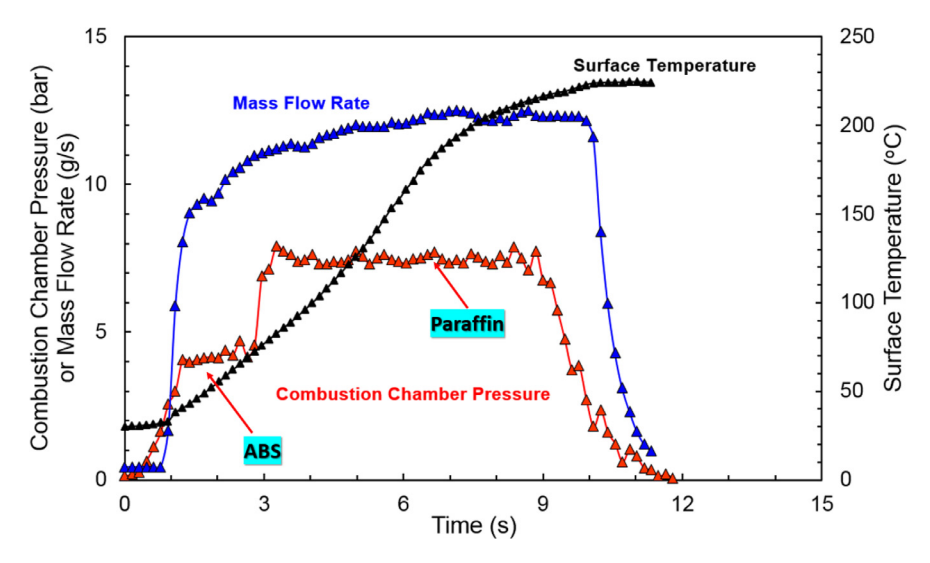


Fig. 7. Typical variations of mass flow rate, combustion chamber pressure and surface temperature over time for the composite fuels.

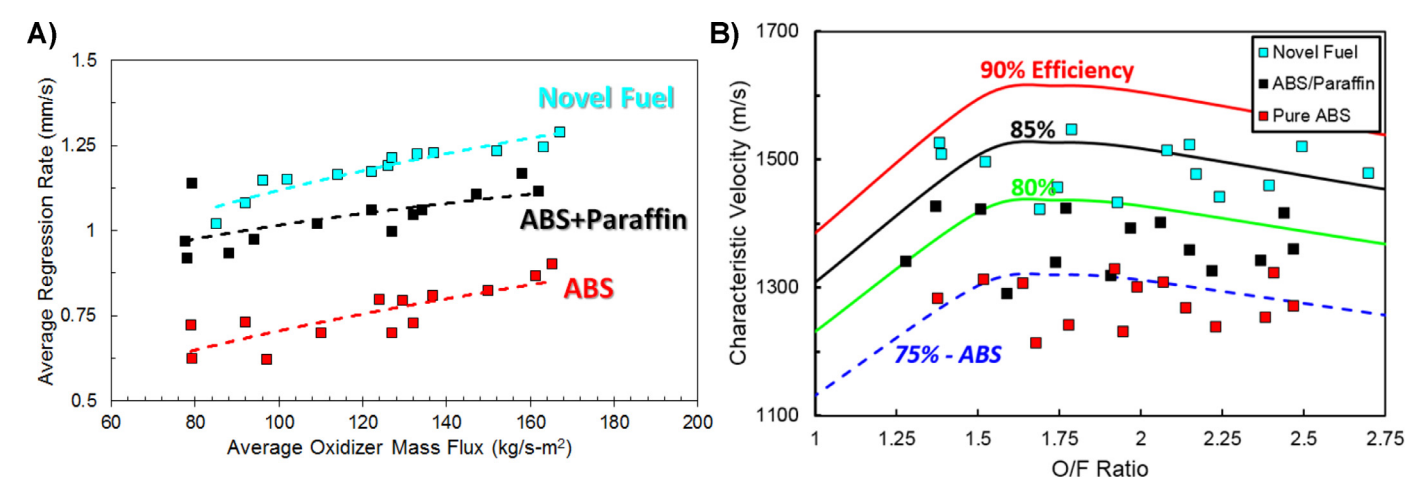


Fig. 8. Ballistic properties of the fuel grains, (a) Comparison of regression rates of CD-doped novel, ABS/paraffin and pure ABS fuel grains, (b) Combustion efficiency of each fuel grain.

both regression rate and combustion efficiency. On the other hand, thanks to the high specific surface area and the presence of additional oxygenic functional groups in CDs, higher O/F ratios during combustion were observed to increase the combustion efficiency [34]. Although the reduction in viscosity due to the macromolecular degradation caused by the oxygenic groups increases the regression rate [35]; it hampers the controlled release of the paraffin particles. The oxygenic groups and high specific surface area of CDs counterbalanced this limitation and increased the heat transferred during combustion. In addition to these, low combustion efficiency of the ABS fuel grains may be ascribed to the rather larger presence of intensive microstructural artifacts such as porosity and poor layer infuse, which are inherent to additive manufacturing.

Conclusions

In this research, the effects of gel-like carbon dots on the combustion properties of ABS + paraffin hybrid rocket fuel grains were investigated. A straightforward and inexpensive multi-step fabrication strategy which involved additive manufacturing of ABS molds followed by casting of neat or CD-doped paraffin was utilized. Pure, fully 3D printed ABS samples were also used as baseline for comparison with the composite fuel grains. The versatile, freeform and adaptable nature of 3D printing allowed rapid production of each type of sample without the need of retooling or post-processing.

After the ballistic tests where gaseous oxygen was used, it was concluded that the addition of gel-like CDs into the paraffin matrix at a ratio of 1% by mass resulted in an enhancement in the regression rate and combustion efficiency values by 11% and 8.5%, respectively, compared to ABS/pure paraffin samples. These enhancements were corroborated via microstructural imaging, rheological and thermal characterizations. SEM images and thermal conductivity characterization evidenced that gel-like CDs formed aggregates with uniform distribution within the paraffin matrix that led to an increase in thermal conductivity due to the thermally more conductive network. Moreover, the viscosity of paraffin matrix was observed to decrease upon introduction of gel-like CDs, which ensured better entrainment of liquid paraffin particles within the combustion flame and higher combustion temperatures, leading to enhanced regression rates. This can be ascribed to the reduction in viscosity through macromolecular degradation within paraffin due to the presence of oxygen groups in CDs. On the other hand, the improvement in combustion efficiency may be attributed to the increase in specific contact surface, presence of the aforementioned oxygenic functional groups and the enhancement in the catalytic activity, as proven by thermogravimetric analysis. Nonetheless, certain reasons like process-induced limitations of 3D printing such as porosity impacted the combustion behavior of all samples, leading to a maximum combustion efficiency of 88% in the novel fuel grain. Although, using a rather larger nozzle with a diameter of 1 mm during the 3D printing step significantly shortened manufacturing time, it led to larger porosity in the ABS matrix, impacting the combustion properties. On the other hand, addition of CDs in the paraffin by 1 wt% compromised the compressive strength by 5%. The promising effects of gel-like CDs on hybrid rocket propulsion may pave the path towards more efficient, larger-scale hybrid rockets for aerospace industry. Future efforts may be devoted on the improvement of mechanical properties of the novel fuel, optimization of carbon dot size and concentration and implementation of structural modifications such as intricate port geometries and multiple ports.

Declaration of Competing Interest

The authors declare no conflict of interest.

Acknowledgments

Professor Roger M. Leblanc thanks the support from National Science Foundation under the grant 011298. Also, authors gratefully acknowledge the great support from King Abdulaziz University, Kingdom of Saudi Arabia, and University of Miami, USA.

Supplementary materials

Supplementary material associated with this article can be found, in the online version, at doi:10.1016/j.combustflame.2020.11.024.

References

- A. Mazzetti, L. Merotto, G. Pinarello, Paraffin-based hybrid rocket engines applications: a review and a market perspective, Acta Astron. 126 (2016) 286–297
- [2] M. Calabro, Overview on hybrid propulsion, Prog. Propuls. Phys. 2 (2011) 353-374.
- [3] M. Chiaverini, Review of solid-fuel regression rate behavior in classical and nonclassical hybrid rocket motors, Prog. Astron. Aeron. 218 (2007) 37.
- [4] B. Cantwell, A. Karabeyoglu, D. Altman, Recent advances in hybrid propulsion, Int. J. Energ. Mater. Chem. Propuls. (2010) 9.
- [5] Z. Wang, X. Lin, F. Li, X. Yu, Combustion performance of a novel hybrid rocket fuel grain with a nested helical structure, Aerosp. Sci. Technol. 97 (2020) 105613
- [6] S. Zhang, F. Hu, W. Zhang, Numerical investigation on the regression rate of hybrid rocket motor with star swirl fuel grain, Acta Astron. 127 (2016) 384–393.
- [7] A.W. Yenawine, Hybrid rocket engines: development of composite fuels with complex 3D printed ports, (2019).
- [8] D. Pastrone, Approaches to low fuel regression rate in hybrid rocket engines, Int. J. Aerosp. Eng. (2012) (2012).
- [9] S.A. Whitmore, S.D. Walker, D.P. Merkley, M. Sobbi, High regression rate hybrid rocket fuel grains with helical port structures, J. Propul. Power 31 (2015) 1727–1738.
- [10] S.A. Whitmore, S.D. Walker, Engineering model for hybrid fuel regression rate amplification using helical ports, J. Propul. Power 33 (2017) 398–407.
- [11] C. Li, G. Cai, H. Tian, Numerical analysis of combustion characteristics of hybrid rocket motor with multi-section swirl injection, Acta Astron. 123 (2016) 26–36.
- [12] J.C. Thomas, E.L. Petersen, J.D. Desain, B. Brady, Hybrid rocket enhancement by micro-and nano-scale additives in HTPB fuel grains, 51st AIAA/SAE/ASEE Joint Propulsion Conference (2015), p. 4041.
- [13] B. Evans, E. Boyer, K. Kuo, G. Risha, M. Chiaverini, Hybrid rocket investigations at penn state university's high pressure combustion laboratory: overview and recent results, 45th AIAA/ASME/SAE/ASEE Joint Propulsion Conference & Exhibit (2009), p. 5349.
- [14] S.C. Sasarita, Hybrid Rocket Motor (HRM) test stand: an investigation of the effects of additives, (2013).

- [15] M.Z. Akhter, M. Hassan, Characterisation of paraffin-based hybrid rocket fuels loaded with nano-additives, J. Exp. Nanosci. 13 (2018) S31–S44.
- [16] H.R. Lips, Experimental investigation on hybrid rocket engines using highly aluminized fuels, J. Spacecr. Rockets 14 (1977) 539–545.
- [17] S.A. Hashim, S. Karmakar, A. Roy, S.K. Srivastava, Regression rates and burning characteristics of boron-loaded paraffin-wax solid fuels in ducted rocket applications, Combust. Flame 191 (2018) 287–297.
- [18] M. Karabeyoglu, D. Altman, B.J. Cantwell, Combustion of liquefying hybrid propellants: part 1, general theory, J. Propul. Power 18 (2002) 610–620.
- [19] G. Di Martino, S. Mungiguerra, C. Carmicino, R. Savino, Computational fluid-dynamic modeling of the internal ballistics of paraffin-fueled hybrid rocket, Aerosp. Sci. Technol. 89 (2019) 431–444.
- [20] M.A. Karabeyoglu, B.J. Cantwell, G. Zilliac, Development of scalable space-time averaged regression rate expressions for hybrid rockets, J. Propul. Power 23 (2007) 737–747.
- [21] S. Chen, Y. Tang, H. Yu, X. Guan, L.T. DeLuca, W. Zhang, R. Shen, Y. Ye, Combustion enhancement of hydroxyl-terminated polybutadiene by doping multiwall carbon nanotubes, Carbon 144 (2019) 472–480.
- [22] M. Kobald, C. Schmierer, H. Ciezki, S. Schlechtriem, E. Toson, L. De Luca, Viscosity and regression rate of liquefying hybrid rocket fuels, J. Propul. Power 33 (2017) 1245–1251.
- [23] X. Xu, R. Ray, Y. Gu, H.J. Ploehn, L. Gearheart, K. Raker, W.A. Scrivens, Electrophoretic analysis and purification of fluorescent single-walled carbon nanotube fragments, J. Am. Chem. Soc. 126 (2004) 12736–12737.
- [24] X. Li, H. Wang, Y. Shimizu, A. Pyatenko, K. Kawaguchi, N. Koshizaki, Preparation of carbon quantum dots with tunable photoluminescence by rapid laser passivation in ordinary organic solvents, Chem. Commun. 47 (2010) 932–934.
- [25] S.Y. Lim, W. Shen, Z. Gao, Carbon quantum dots and their applications, Chem. Soc. Rev. 44 (2015) 362–381.
- [26] Q. Qu, A. Zhu, X. Shao, G. Shi, Y. Tian, Development of a carbon quantum dot-s-based fluorescent Cu 2+ probe suitable for living cell imaging, Chem. Commun. 48 (2012) 5473–5475.
- [27] X. Wu, Y. Song, X. Yan, C. Zhu, Y. Ma, D. Du, Y. Lin, Carbon quantum dots as fluorescence resonance energy transfer sensors for organophosphate pesticides determination, Biosens. Bioelectron. 94 (2017) 292–297.
- [28] Z. Wang, Z. Dai, Carbon nanomaterial-based electrochemical biosensors: an overview, Nanoscale 7 (2015) 6420–6431.
- [29] P.G. Luo, S. Sahu, S.-.T. Yang, S.K. Sonkar, J. Wang, H. Wang, G.E. LeCroy, L. Cao, Y.-.P. Sun, Carbon "quantum" dots for optical bioimaging, J. Mater. Chem. B 1 (2013) 2116–2127.
- [30] Y. Wang, L. Chen, Quantum dots, lighting up the research and development of nanomedicine, Nanomedicine: nanotechnology, Biol. Med. 7 (2011) 385–402.
- [31] E. Celik, C. Oztan, Y. Zhou, R. LeBlanc, O. Genc, S. Ballikaya, Enhancement of thermoelectric figure of merit of Bi₂Te₃ using carbon dots, ASME 2018 International Mechanical Engineering Congress and Exposition, American Society of Mechanical Engineers Digital Collection, 2018.
- [32] Y. Zhou, K.J. Mintz, C.Y. Oztan, S.D. Hettiarachchi, Z. Peng, E.S. Seven, P.Y. Liyanage, S. De La Torre, E. Celik, R.M. Leblanc, Embedding carbon dots in superabsorbent polymers for additive manufacturing, Polymers 10 (2018) 921.
- [33] X. Chen, H. Gao, M. Yang, W. Dong, X. Huang, A. Li, C. Dong, G. Wang, Highly graphitized 3D network carbon for shape-stabilized composite PCMs with superior thermal energy harvesting, Nano Energy 49 (2018) 86–94.
- [34] E. Ettefaghi, B. Ghobadian, A. Rashidi, G. Najafi, M.H. Khoshtaghaza, M. Rashtchi, S. Sadeghian, A novel bio-nano emulsion fuel based on biodegradable nanoparticles to improve diesel engines performance and reduce exhaust emissions, Renew. Energy 125 (2018) 64–72.
- [35] M.A. Haruna, Z. Hu, H. Gao, J. Gardy, S.M. Magami, D. Wen, Influence of carbon quantum dots on the viscosity reduction of polyacrylamide solution, Fuel 248 (2019) 205–214
- [36] Y. Ji, Y. Zhou, E. Waidely, A. Desserre, M.H. Marksberry, C.C. Chusuei, A.A. Dar, O.A. Chat, S. Li, R.M. Leblanc, Rheology of a carbon dot gel, Inorgan. Chim. Acta 468 (2017) 119–124.
- [37] A. Bath, Performance characterization of complex fuel port geometries for hybrid rocket fuel grains, (2012).
- [38] M. Creech, A. Crandell, N. Eisenhauer, S. Marx, T. Busari, A. Link, J. Gabl, T.L. Pourpoint, 3D printer for paraffin based hybrid rocket fuel grains, 53rd AIAA Aerospace Sciences Meeting (2015), p. 0924.
- [39] M. McFarland, E. Antunes, Small-scale static fire tests of 3D printing hybrid rocket fuel grains produced from different materials, Aerospace 6 (2019) 81.
- [40] C. Paravan, L. Galfetti, R. Bisin, F. Piscaglia, Combustion processes in hybrid rockets, Int. J. Energ. Mater. Chem. Propulsion (2019) 18.
- [41] S. Gordon, B.J. McBride, Computer program for calculation of complex chemical equilibrium compositions and applications. Part 1, Analysis (1994).